Transactions of the Korean Nuclear Society Virtual Autumn Meeting
December 17-18

The Size Effect of Powdered Scintillator on High-Resolution X-ray Imaging System

Heon Yong Jeong [a], Ju Hyuk Lee [a], Jun Heo [a] and Sung Oh Cho [a*]
[a]*Nuclear and Quantum Eng., KAIST, 291, Daehak-ro, Yuseong-gu, Daejeon, Republic of Korea*
[*]*Corresponding author: socho@kaist.ac.kr*

1. Introduction

Digital X-ray imaging uses a converter which emits visible light (indirect) or electrons (direct) when absorbing X-ray. Indirect system uses a scintillator as a converter with light detector [1-4]. A scintillator is a substance that emits visible light when it reacts with X-ray or other radiations. The structure and optical properties of scintillators affect the quality of X-ray images. Powdered-scintillator screen for X-ray image is used a lot in industry, medical diagnostics and various fields [5-9]. In such a scintillator, the optical light generated from the scintillator is optically diffused by other grains, resulting in light spread, which reduces the spatial resolution of X-ray image [10-12]. However, if nanoparticle scintillators are used for powdered-scintillator screen, high spatial resolution can be achieved due to low light spread [13, 14]. In this experiment, powdered zinc tungstate ($ZnWO_4$) scintillators were prepared by the solid-state reaction. $ZnWO_4$ is of great interest as ultraviolet, X-ray, ɣ -ray, electron beam and proton beam scintillator [15-19]. For the above reasons, $ZnWO_4$ has the unique characteristics about luminescent property, high density, high chemical stability, short decay time, low afterglow, and economical price [16, 20-25].

Meanwhile, my research team developed the high-resolution X-ray inspection system (HRXIS) [26]. This system consists of a carbon nano-tube (CNT) based miniature x-ray tube, a scintillator, an optical lens, and a scientific complementary metal-oxide-semiconductors (sCMOS) detector. The concept of the developed system is that transmits the X-ray in the form of an object attached to a scintillator, and then magnifies the image formed on the scintillator screen using an optical lens, then acquire images on the sCMOS detector. This system not only can acquire X-ray images with high spatial resolution, but also inspect the internal defect of micro-sized small objects.

In this study, the zinc oxide nanoparticles and tungsten oxide nanoparticles used in the solid-state reaction were synthesized using anodization method. Anodization method is that if a platinum relative electrode (-) and a metal wire (+) are added to the electrolyte and then a voltage of 10-100 V are applied, oxidation and etching occurs on the metal wire resulting in metal oxide nanoparticles [27]. $ZnWO_4$ nanoparticles were fabricated through the solid-state reaction using as-prepared zinc oxide nanoparticles and tungsten oxide nanoparticles. The solid-state reaction was carried out at different temperatures for fabricating the various sizes of $ZnWO_4$ powders. The different sizes of $ZnWO_4$ powders were fabricated as thin screens on silicon glasses. These scintillator screens were applied to the HRXIS for obtaining X-ray image. Finally, it was evaluated whether high spatial resolution of X-ray images can be obtained when nanoparticle scintillators are applied to high-resolution X-ray imaging.

2. Materials and Methods

2.1 Materials

We purchased zinc wires and tungsten wires from Goodfellow (Huntingdon, UK). Potassium chloride (KCl) powder, ammonium fluoride (NH_4F) powder and polyethylene glycol (PEG, average molecular wight 200) were purchased from Sigma-Aldrich (St Louis, Missouri, USA).

2.2 Characterization of $ZnWO_4$

The zinc oxide nanoparticles and the tungsten oxide nanoparticles were synthesized by anodization method. The electrolytes were made by adding 1M KCl and 1M NH_4F respectively to deionized (DI) water. The zinc oxide nanoparticles were synthesized by applying 15 V to zinc wires in the electrolyte of 1M KCl. In case of tungsten oxide nanoparticles, the voltage of 80 V was applied in 1M NH_4F. Both nanoparticles were washed with DI water and were dried at 60°C in air. Both nanoparticles with 1:1 atomic ratio of zinc and tungsten were added in DI water with 0.2 wt% PEG and mixed well with the sonication and vibrating ball milling, and then this aqueous solution was dried at 60°C in air. A solid-state reaction was implemented in electric furnace at different temperatures with 700, 800, and 900°C for 1 hour.

The nano-structures of zinc oxide nanoparticles and tungsten oxide nanoparticles were observed by a transmission electron microscope (TEM, Titan cubed G2 60-300, FEI, Hillsboro, OR, USA). The structures of $ZnWO_4$ powders were observed by FE-SEM. The crystalline structures of $ZnWO_4$ powders were analyzed by high-resolution X-ray diffraction (HR-XRD, SmartLab, Rigaku, Tokyo, Japan) with an analysis 2θ range 10-90°.

2.3 Fabrication of $ZnWO_4$ scintillator screen

The $ZnWO_4$ scintillator screens on the 150 μm silicon glass (1.5 cm x 1.5 cm) were made by drop casting method. $ZnWO_4$ powders, PEG, and DI water were prepared to make $ZnWO_4$ paste. After adding $ZnWO_4$ powder into DI water with 0.2 wt% PEG, this paste was ball-milled for 1 hours. Finally, $ZnWO_4$ paste was put on silicon glass and made to a 10 μm thin screen by adjusting the concentration of $ZnWO_4$ powders. The $ZnWO_4$ scintillator screens were applied to HRXIS for obtaining X-ray images and evaluating the spatial resolution of the X-ray images.

3. Result and Discussion

3.1 Nanoparticles synthesized by anodization

The Zinc oxide nanoparticles and tungsten oxide nanoparticles were prepared by anodization method. Figure. 1(a) is the image of zinc oxide nanoparticles acquired by TEM. This figures demonstrate that the zinc oxide nanoparticles are spherical and sized in 20-40 nm. The TEM image of tungsten oxide nanoparticles is shown in Figure. 1(b). This images show that tungsten oxide nanoparticles are in the form of nano-plate with a width of 20-60 nm.

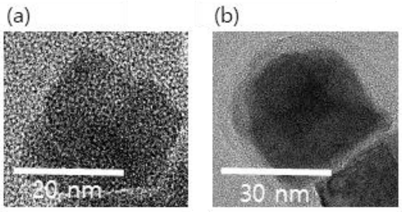

Fig. 1. Metal oxide nanoparticles synthesized by anodization method, (a) TEM image of zinc oxide nanoparticles, and (b) TEM image of tungsten oxide nanoparticles

3.2 Structure of $ZnWO_4$ scintillator

The $ZnWO_4$ powders were fabricated by solid-state reaction at different temperature at 700, 800 and 900°C. The structure morphology of $ZnWO_4$ powders are showed in Figure. 2(a)-(c) by FE-SEM. The $ZnWO_4$ powders were sized through FE-SEM. As a result, the average sizes of powders fabricated at 700, 800, and 900°C were 176.4 nm, 626.7 nm, and 2.127 μm respectively. The $ZnWO_4$ powders fabricated at 700°C and 800°C were formed in the wavelength band of light or smaller. However, the size of the powders fabricated at 900°C were formed to micro-sized particles larger than the wavelength of light. Figure. 2(d) shows the XRD patterns of the $ZnWO_4$ powders with an analysis 2θ range 10-90o. Comparing the peak value of the XRD pattern with the standard card (PDF ICDD card #01-078-0251), these powders were crystallized into pure monoclinic $ZnWO_4$.

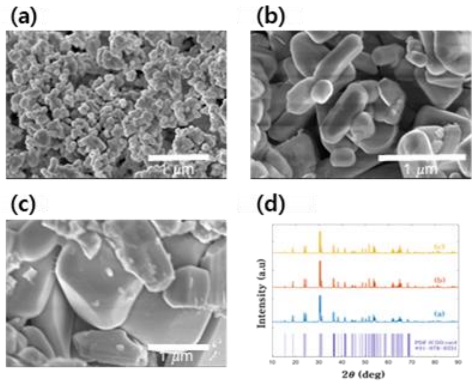

Fig. 2. FE-SEM image of $ZnWO_4$ fabricated at (a) 700°C, (b) 800°C, and (c) 900°C, (d) XRD pattern of $ZnWO_4$.

3.3 Evaluation of X-ray imaging performance in HRXIS

The $ZnWO_4$ scintillator screens were prepared on silicon glass by drop casting method. Fabricated scintillator screens were applied to HRXIS (Figure. 3). This system consists of a miniature X-ray tube, a 10x optical lens, and a sCMOS detector. The miniature X-ray tube was produced directly in our lab [28]. This X-ray tube is composed of carbon nano-tube(CNT) based electron beam emitter, the tube voltage is 50 kVp and the current is 0.35 mA. This X-ray tube is equipped with focusing lens. The focusing lens is a cylindrical form composed of permanent magnets. The focal spot of the miniature X-ray tube using focusing lens was 337-390 um [26]. A 10x optical lens and a sCMOS detector were used to magnify and obtain images on scintillators. The pixel size of the sCMOS detector is 6.5 um. When the image on scintillator is magnified by a 10x optical lens, the effective pixel size is 0.65 um.

Fig. 3. Applying $ZnWO_4$ scintillator screen to HRXIS

The modulation transfer function (MTF) was measured to evaluate the spatial resolution according to the size of $ZnWO_4$ powders. The MTF is a general method to analyze the spatial resolution of X-ray image [13, 26, 29-30]. A 0.5 cm thick tungsten block was placed on the fabricated $ZnWO_4$ scintillator screen and the X-ray image for edge of tungsten block were obtained using HRXIS. The edge spread function (ESF) was determined through the obtained X-ray image, and the ESF was converted to MTF. The MTF curve of each scintillator screen is shown in Figure. 4. The spatial frequency (lp/mm) was evaluated at 10% of the MTF. The spatial frequency of the scintillator screens with an average particle size of 176.4 nm, 626.7 nm, and 2.127 μm were 278.2, 204.1, and 124.1 lp/mm. As a result, high spatial resolution of X-ray images can be acquired with a scintillator screen composed of nano-sized particles.

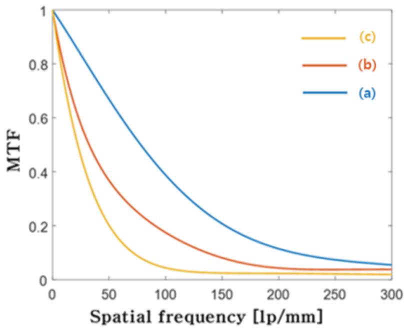

Fig. 4. MTF curve of scintillator screen composed of $ZnWO_4$ powders with different averaged sizes of (a) 176.4 nm, (b) 626.7 nm, and (c) 2.127 μm.

4. Conclusion

The $ZnWO_4$ scintillator powders were fabricated by a convenient way using the anodization method and the solid-state reaction. These $ZnWO_4$ scintillator powders were fabricated in the form of scintillator screens and applied to high-resolution X-ray imaging for evaluating spatial resolution of X-ray image. The result showed that the spatial resolution would be optimized if the average diameter of the particle was less than the wavelength of light in powdered-scintillator screen. These results proved that the $ZnWO_4$ nanoparticle scintillator can be utilized for obtaining X-ray images with high spatial resolution.

A commercialized powered scintillator is micro-sized particles larger than the wavelength of light [14]. However, the result of this experiment showed that scintillators with the size of 100-250 nm generate less light diffusion, thus improving the spatial resolution of the X-ray images. This study will have an impact on a lot of research about powdered-scintillator screens. This result can be applied not only to $ZnWO_4$ scintillator, but also to other scintillator materials, so this experiment will be of sufficient help to study other nanoparticle scintillator materials.

REFERENCES

1. Nagarkar, V.V., et al., Structured CsI(Tl) scintillators for X-ray imaging applications. IEEE transactions on nuclear science, 1998. 45(3): p. 492-496.
2.Smith, K., et al., Nanophosphor-based contrast agents for spectral X-ray imaging. Nanomaterials, 2019. 9(8): p. 1092.
3. Chen, Q., et al., All-inorganic perovskite nanocrystal scintillators. Nature, 2018. 561(7721): p. 88-93.
4. Lempicki, A., et al., A new lutetia-based ceramic scintillator for X-ray imaging. Nuclear Instruments & Methods in Physics Research Section a-Accelerators Spectrometers Detectors and Associated Equipment, 2002. 488(3): p. 579-590.
5. Michail, C., et al., Measurement of the luminescence properties of Gd2O2S: Pr, Ce, F powder scintillators under X-ray radiation. Radiation measurements, 2014. 70: p. 59-64.
6. Rowlands, J., The physics of computed radiography. Physics in Medicine & Biology, 2002. 47(23): p. R123.
7. Michail, C., et al., Evaluation of the imaging performance of LSO powder scintillator for use in X-ray mammography. Nuclear Instruments and Methods in Physics Research Section A: Accelerators, Spectrometers, Detectors and Associated Equipment, 2007. 580(1): p. 558-561.
8. Adam, J., et al., Light emission intensities of luminescent Y2O3: Eu and Gd2O3: Eu particles of various sizes. Nanomaterials, 2017. 7(2): p. 26.
9. V.V.Nagarkar, et al., A new large area scintillator screen for X-ray imaging. Nuclear Instruments and Methods in Physics Research Section B: Beam Interactions with Materials and Atoms, 2004. 213: p. 250-254.
10. Poludniowski, G.G. and P.M. Evans, Optical photon transport in powdered-phosphor scintillators. Part 1. Multiple-scattering and validity of the Boltzmann transport equation. Medical Physics, 2013. 40(4): p. 041904.
11. Chen, G., et al., Fluorozirconate-based nanophase glass ceramics for high-resolution medical X-ray imaging. Journal of non-crystalline solids, 2006. 352(6-7): p. 610-614.
12. Ohashi, Y., et al., Submicron-diameter phase-separated scintillator fibers for high-resolution X-ray imaging. Applied Physics Letters, 2013. 102(5): p. 051907.
13. Cha, B.K., et al., Characterization and imaging performance of nanoscintillator screen for high resolution X-ray imaging detectors. Nuclear Instruments and Methods in Physics Research Section A: Accelerators, Spectrometers, Detectors and Associated Equipment, 2011. 633: p. S294-S296.
14. Liaparinos, P.F., Optical diffusion performance of nanophosphor-based materials for use in medical imaging. Journal of biomedical optics, 2012. 17(12): p. 126013.
15. Zhai, B.-g., L. Yang, and Y.M. Huang, Intrinsic Defect Engineering in Eu3 Doped ZnWO4 for Annealing Temperature Tunable Photoluminescence. Nanomaterials, 2019. 9(1): p. 99.
16. Kraus, H., et al., Feasibility study of a ZnWO4 scintillator for exploiting materials signature in cryogenic WIMP dark matter searches. Physics Letters B, 2005. 610(1-2): p. 37-44.
17. Klamra, W., et al., Properties of CdWO4 and ZnWO4 scintillators at liquid nitrogen temperature. Journal of Instrumentation, 2012. 7(03): p. P03011.
18. Chernov, S., et al., Luminescence spectra and decay kinetics in ZnWO4 and CdWO4 crystals. physica status solidi (b), 2004. 241(8): p. 1945-1948.
19. Kang, S.J., et al., Scintillation properties and luminescence response of the ZnWO 4 crystal to γ and proton

beams. Journal of the Korean Physical Society, 2013. 63(7): p. 1466-1472.
20. Fu, H., et al., Photocatalytic activities of a novel ZnWO4 catalyst prepared by a hydrothermal process. Applied Catalysis A: General, 2006. 306: p. 58-67.
21. Lou, Z., J. Hao, and M. Cocivera, Luminescence of ZnWO4 and CdWO4 thin films prepared by spray pyrolysis. Journal of luminescence, 2002. 99(4): p. 349-354.
22. Wang, K., et al., Synthesis and photoluminescence of novel red-emitting ZnWO4: Pr3+, Li+ phosphors. Spectrochimica Acta Part A: Molecular and Biomolecular Spectroscopy, 2016. 154: p. 72-75.
23. Ryu, J.H., C.S. Lim, and K.H. Auh, Synthesis of ZnWO4 nanocrystalline powders, by the polymerized complex method. Materials Letters, 2003. 57(9-10): p. 1550-1554.
24. Wen, F.-S., et al., Hydrothermal synthesis and photoluminescent properties of ZnWO4 and Eu3+-doped ZnWO4. Materials Letters, 2002. 55(3): p. 152-157.
25. Dkhilalli, F., et al., Structural, dielectric, and optical properties of the zinc tungstate ZnWO 4 compound. Journal of Materials Science: Materials in Electronics, 2018. 29(8): p. 6297-6307.
26. Kim, H.N., et al., Development of a high resolution x-ray inspection system using a carbon nanotube based miniature x-ray tube. Review of Scientific Instruments, 2020. 91(4): p. 043703.
27. Ali, G., et al., A Green, General, and Ultrafast Route for the Synthesis of Diverse Metal Oxide Nanoparticles with Controllable Sizes and Enhanced Catalytic Activity. ACS Applied Nano Materials, 2018. 1(11): p. 6112-6122.
28. Heo, S.H., et al., A vacuum-sealed miniature X-ray tube based on carbon nanotube field emitters. Nanoscale research letters, 2012. 7(1): p. 1-5.
29. Rossmann, K., Measurement of the modulation transfer function of radiographic systems containing fluorescent screens. Physics in Medicine & Biology, 1964. 9(4): p. 551.
30. Gambaccini, M., et al., MTF evaluation of a phosphor-coated CCD for x-ray imaging. Physics in Medicine & Biology, 1996. 41(12): p. 2799.